Near-infrared imaging of the environment of 6.7-GHz methanol masers

S. Goedhart,[1,2]★ D. J. van der Walt[2] and M. J. Gaylard[1]

[1]*Hartebeesthoek Radio Astronomy Observatory, PO Box 443, Krugersdorp, 1740, South Africa*
[2]*Space Research Unit, Physics Department, Potchefstroom University for CHE, Private Bag X6001, Potchefstroom, 2520, South Africa*

ABSTRACT

Near-infrared (NIR) images at I, J, H and K bands were made of 12 southern 6.7-GHz methanol maser sources. Astrometry accurate to 0.5 arcsec was obtained. The positions of known H II regions, water masers, hydroxyl masers, and mid- and far-infrared objects in the region are examined in order to try to determine the nature of the methanol maser source. Deeply embedded NIR sources were found close to seven out of 14 maser sites. In three cases, no NIR source, H II region, water maser or hydroxyl maser could be found in likely association with the methanol masers.

Key words: masers – ISM: clouds – H II regions – infrared: ISM – radio lines: ISM.

1 INTRODUCTION

Massive stars have a significant impact on the interstellar medium (Leitherer, Robert & Drissen 1992), therefore it is vital for the understanding of the evolution of the Galaxy to study the life cycles of massive stars. Since massive stars in their earliest evolutionary phases are deeply embedded in their natal molecular cloud, it is not possible to observe them directly at optical wavelengths. However, it is possible to study such stars indirectly by their effects on the surrounding dust and gas. The embedded stars can ionize the surrounding gas, giving rise to ultracompact (UC) H II regions. The radiation from the star will be absorbed by the surrounding dust and will be reradiated at infrared wavelengths. Winds from the star can also set up shocks. The interaction of the star with its surrounding cloud can thus produce conditions favourable for the existence of masers.

Methanol masers, hydroxyl masers and water masers are found near sites of massive star formation (Garay & Lizano 1999). Extensive surveys have been carried out to detect class II methanol masers at 6.7 and 12.2 GHz (e.g. Caswell et al. 1995a,b), hydroxyl masers (e.g. Caswell 1998), water masers (e.g. Brand et al. 1994) and UC H II regions (e.g. Becker et al. 1994) in the Galaxy. These radio phenomena occur in different parts of the environment around the exciting star. Therefore, examination of their positions relative to each other can give us an indication of the conditions surrounding the star.

At present, the conditions giving rise to methanol masers are not well understood. Hypotheses have been advanced suggesting that the methanol masers occur in circumstellar discs (Norris et al. 1998; Minier, Booth & Conway 2000). However, there are a significant number of masers that do not appear to conform to these theories (Phillips et al. 1998). It is possible that methanol masers are found in outflows, bow shocks or other areas in the star formation regions. Infrared images can show us the positions of embedded stars in the region, as well as give an indication of the disposition of the dust and gas relative to the positions of the masers.

Although other workers have imaged massive star formation regions, the emphasis has not been on methanol masers. However, some of the water maser sources imaged in the J, H and K bands by Testi et al. (1994, 1998) also have 6.7-GHz methanol masers associated with them. Osterloh, Henning & Launhardt (1997) imaged 31 cold southern *IRAS* (1985) sources at H and K'. None of these studies considered the position of methanol masers relative to near-infrared (NIR) objects in each region. Walsh et al. (1999) imaged 25 methanol maser sources at J, H, K and L bands with a limiting magnitude of 14 at all bands under conditions that may not have been photometric. Their astrometry had uncertainties ranging from 2 to 4 arcsec.

We present near-infrared images of the regions surrounding 12 6.7-GHz methanol maser sites. These sources were selected from the list of methanol maser sources being monitored for variability at Hartebeesthoek Radio Astronomy Observatory. Seven of the sources presented in this paper are not known to have been imaged previously at NIR wavelengths. In this paper we examine the relation of the methanol masers to NIR objects, H II regions and other maser species. The large field of view used enabled us to obtain astrometry accurate to 0.5 arcsec and gives us an indication of whether the field around the methanol masers differs from other areas. The details of the observations and reductions will be given in Section 2. In Section 3 the results are presented. We discuss the sources in detail in Section 4 and discuss our findings in Section 5. Our summary is presented in Section 6.

2 OBSERVATIONS AND DATA REDUCTION

The observations were made using the OSIRIS camera on the 1.5-m telescope at Cerro Tololo Inter-American Observatory on the

Table 1. Central wavelengths of filters.

Filter	I	J	H	K
λ (μm)	0.90	1.22	1.65	2.18

nights of 1999 July 29 to August 1. The camera used a 1024×1024 HgCdTe detector with a plate scale of 0.46 arcsec pixel^{-1} and a central illuminated area corresponding to 266 arcsec at a focus of $f/13.5$.

Images were made at I, J, H and K bands. Table 1 gives the wavelengths of the filters. Eight co-adds of 3 s each were used for each exposure. The shortest possible exposure time for the co-adds was selected to try to avoid saturating the detector. Four dithered images each were taken at I, J and H bands and eight images were made at K band for each object. In cases where the fields were difficult to identify, additional images at I band were taken with the telescope centred on nearby bright stars – normally *HST* guide stars – in such a way that there was overlap with the on-source image. Standard stars from the list of faint standards of Persson et al. (1998) were observed at regular intervals. The detection limits at J, H and K were found to be a maximum of 16 mag. However, as will be shown later, the sensitivity limit may have varied in individual fields. In some images the faintest object detected at H or K band was 14.5 mag.
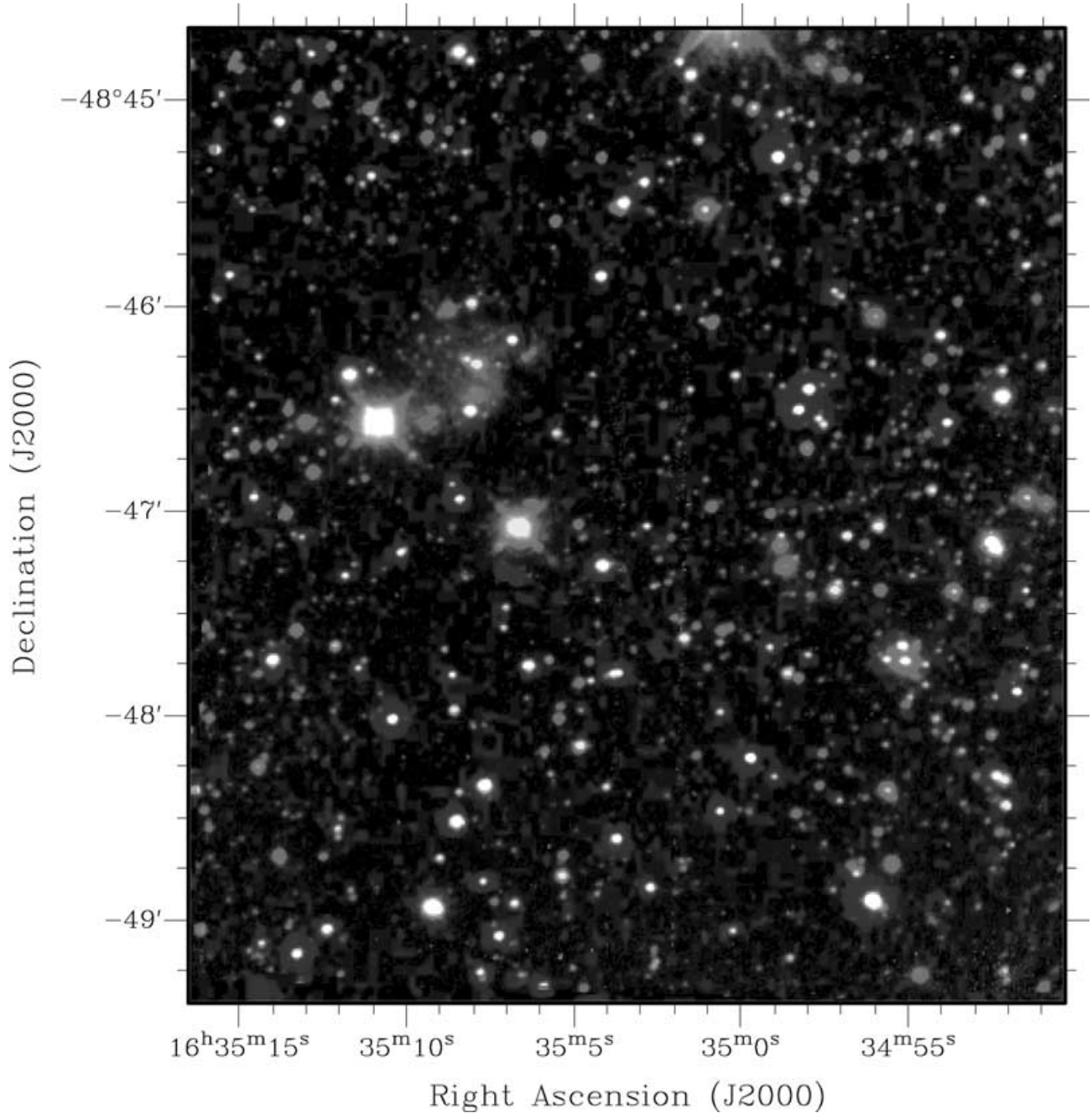

Figure 1. Three-colour composite image showing overlap between optical and infrared sources for G336.01−0.82. This figure is available in colour on *Synergy*, the online version of the journal, where the blue frame is the Digitized Sky Survey field, the green frame is the *I*-band image and the red frame is the *K*-band image.

Table 2. *J*-, *H*- and *K*-band magnitudes and flux densities of infrared objects close to the methanol maser positions.

No	Methanol source	RA (J2000)	Dec. (J2000)	J (mag)	F_J (mJy)	H (mag)	F_H (mJy)	K (mag)	F_K (mJy)
1	G10.33−0.17 B	18 09 01.632	−20 05 07.25	–	–	–	–	10.93	28.14
2	G10.33−0.17 C	18 08 55.723	−20 05 57.37	–	–	12.76	8.46	11.26	20.76
3	G12.91−0.26	18 14 39.595	−17 52 01.38	14.58	2.67	12.55	10.29	8.79	202.00
4	G45.07+0.13 no 1	19 13 22.089	10 50 55.59	–	–	–	–	10.10	60.43
5	G45.07+0.13 no 2	19 13 21.876	10 50 50.36	–	–	–	–	10.52	41.04
6	G52.67−1.09 no 1	19 32 36.091	16 57 40.02	–	–	13.24	5.44	10.83	30.85
7	G52.67−1.09 no 2	19 32 36.182	16 57 32.30	–	–	15.15	0.94	12.70	5.51
8	G328.81+0.63	15 55 48.571	−52 43 11.46	–	–	–	–	10.91	28.66
9	G337.92−0.46	16 41 06.111	−47 06 58.29	–	–	12.60	9.82	10.71	34.45
10	G339.62−0.12	16 46 06.101	−45 36 41.58	–	–	12.18	14.46	9.67	89.79
11	G351.78−0.54	17 26 42.910	−36 09 13.39	–	–	–	–	11.17	22.56

The data reductions were done using IRAF. The detector being used on OSIRIS at that time had a bias discontinuity across the quadrants of the detector that could not be subtracted completely using the overscan area, or removed using dome flats. The bias appeared to vary slowly with time. To address this, sky fields were constructed by median averaging the standard star fields observed before and after the program field. The field that cleanly subtracted the bias was then adopted as the sky field. The averaged sky fields for the night were used to make a flat-field. This results in a very clean image with most of the bias removed. The final composite images were made using the SQMOS and NIRCOMBINE tasks in the NOAO SQIID package.

The solution of the image world coordinate system was found using images from the Digitized Sky Survey (DSS) as reference fields. The *I*-band images were invaluable in identifying NIR counterparts to some of the faint optical stars. In all cases, it was possible to find stars visible in all bands and register the images directly to the DSS image, which ensured that no cumulative errors occured from finding solutions in a stepwise manner. Fig. 1 shows the overlap in sources at *V*, *I* and *K* bands for a typical field. Owing to the crowded nature of the infrared fields in the vicinity of the methanol masers, an accurate coordinate transform was vital for comparing the NIR environment with the methanol maser positions. Typically, at least 15 reference stars spaced around the entire field were used to obtain the coordinate transform. The rms error of the WCS solution was of the order of 0.5–0.7 arcsec. This level of positional uncertainty is of the same order as the absolute positional uncertainty of the methanol maser spots, so it is possible to compare maser positions and NIR objects in a meaningful manner at this level, unless there are multiple stars less than 0.5 arcsec from each other.

The IRAF DAOPHOT package was used to obtain the photometry of the sources. It was found that some of the *K*-band sources near methanol masers were not point sources, i.e. their profile did not match that of the point spread function found using field stars on the same image. Therefore, fluxes obtained using DAOPHOT and the point spread function may be underestimated. It was decided to estimate the fluxes of these sources using simple aperture photometry techniques instead.

3 RESULTS

The general trend observed here is for the environment of the methanol masers to be very crowded. This is not surprising since it is well known that massive stars tend to form in clusters. These sources are situated along the galactic plane, hence there are many unrelated stars adding to the crowded fields. At this time, observational evidence suggests that the methanol masers trace objects in a very early evolutionary phase (Walsh et al. 1999; Minier, Conway & Booth 2001), therefore we may expect that the sources will be deeply embedded and highly reddened as a result. Deeply embedded sources would have steep spectral energy distributions (SEDs) decreasing towards shorter wavelengths (Goedhart, van der Walt & Schutte 2000). If the optical depth of the cloud is high, the embedded source may only be detectable at *K* band, if it can be detected at all. In contrast, main-sequence stars would have a SED that decreases toward longer wavelengths and would therefore appear bluer than an embedded star. Visual examination of the distribution of stars with different colours in the field around the methanol masers shows that stars with blue colours or slightly reddened main-sequence stars are distributed fairly uniformly over the image. This suggests that these are foreground stars and stars that are reddened by normal interstellar extinction. We can therefore safely disregard these stars in our analysis.

The positions, magnitudes and flux densities[1] of objects likely to be deeply embedded sources, within 10 arcsec of the methanol masers, are listed in Table 2. Fig. 2 shows the position of these sources on a $J - H$ versus $H - K$ two-colour diagram. The only source visible at all three bands is G12.91−0.26, which has an infrared excess. It is not possible to tell whether the other sources are simply deeply embedded or whether they have an infrared excess since *J* magnitudes are not available. The majority of these sources have $H - K > 1.5$. If we assume that the sources do not have an infrared excess, this implies that the extinction caused by dust is greater than 5 mag. In the more extreme cases where $H - K > 3$ the extinction would be greater than 7 mag.

How common are such sources in the fields imaged? Fig. 3 shows plots of *K* magnitude against $H - K$ colour in each field imaged for all sources visible at *H* and *K* bands only. We do not use a two-colour diagram because it was found that the observed colours of some very bright sources placed these stars above the reddening band in a $J - H$ versus $H - K$ diagram. Such colours are unrealistic (Lada & Adams 1992), indicating a possible observational problem. Investigation found that these sources were typically very bright and showed evidence of 'blooming'. This problem was not found for fainter sources visible only at *H* and *K* bands. In order to exclude sources with such saturation effects when examining the entire field, we look at *K* versus $H - K$ diagrams for sources that were

[1] A description of the method used to obtain the zero points for the LCO system is given in Appendix A.
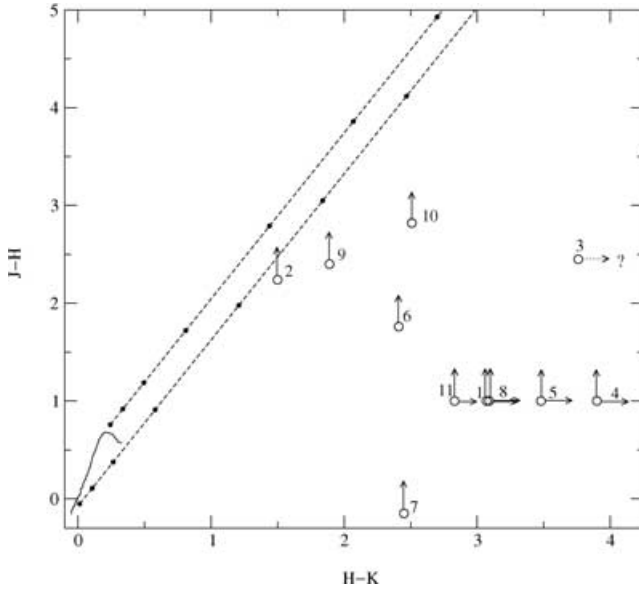
Figure 2. $H - K$ versus $J - K$ diagram of the stars possibly associated with methanol masers. The solid line shows the colours of the unreddened main-sequence stars (Koorneef 1983). The dashed lines indicate the reddening band (Rieke & Lebofsky 1985), within which reddened main-sequence stars should lie. Filled circles are placed at intervals of 1 mag of extinction along the reddening vectors. The open circles are enumerated according to the source numbers given in Table 2. The arrows indicate that the colours plotted are lower limits. Objects 1, 4, 5, 8 and 11 have a K-band mag. alone. Upper limits of 16 mag at J and 15 mag at H are assumed. Object 3 may have been saturated in the K band.

only detected at H and K bands. This does not affect our analysis significantly since the majority of the saturated stars belong to the group that we decided to exclude, as discussed above. It can be seen that the sources listed in Table 2 are typically among the brightest of the K-band sources. This makes it less probable that these objects are just associated with the methanol maser by chance. The sources with measurable $H - K$ colours appear to fall below a line on the diagram that defines the limiting magnitude at H. The limiting magnitudes for each image were determined by inspection. This limiting magnitude ranged from 14.5 to 16 and did not appear to be dependent on airmass. It is possibly an effect of the time variable bias mentioned earlier.

Three-colour composite images[2] of the J, H and K bands are presented in Figs 4–15 in Section 4. Although only the area immediately around the masers is discussed in detail in this paper, we present the full 266 arcsec fields since they may be of use as finding charts for other workers. Examination of the large field also gives an indication of the stellar environment, e.g. we can determine the probability of confusion in the area around the maser source. Enlarged images of the area of interest around each methanol maser group are also presented. The positions of known H II regions (○), water masers (∗), 6.7-GHz methanol masers (+) and hydroxyl masers (×) are marked on the images. The ellipses show the *IRAS* error box in the cases where there is an *IRAS* point source in the field of view. The white contours are the Midcourse Space Experiment (MSX) A-band (8-μm) intensities (Price et al. 2001). The MSX survey has a spatial resolution of 18 arcsec.

[2] The RGB images and contour overlays were produced using the KARMA package (Gooch 1996).

Table 3 lists the positions of the observed radio emitters and the reference to the paper reporting the most accurate position. Where multiple maser spots are present, the centroid position for each group is tabulated. The kinematic distances for the maser sources are given in Table 4. Table 5 gives the separations between the other objects in the field and the methanol masers, using the near kinematic distance. In the following sections we examine the area around each methanol maser site in detail.

4 NOTES ON INDIVIDUAL SOURCES

4.1 G10.33−0.17

In this field, four separate groups of maser spots occur (Fig. 4). Unfortunately one of the groups lies just outside the field of view of the camera owing to a small drift in the telescope centring. Although the spot groups have similar velocities, they have a significant spatial separation (∼100 arcsec, see Table 5). Using a kinematic distance of 2.2 kpc, the greatest separation (projected on the plane of the sky) between the maser sites is of the order of 1.5 pc. This implies that the different spot groups are being powered by different embedded stars, but they probably belong to the same molecular cloud. The MSX images show an arc of emission, with unresolved sources visible at two of the three maser sites.

The maser site in the northern part of the field (referred to as G10.33−0.17 A, Fig. 4b) is in a dark region of the cloud. There are no bright K-band objects, H II regions or other maser species in this area. There is very faint diffuse emission at K-band 4 arcsec to the north of the methanol maser position. This object is too faint to obtain a reliable magnitude estimate. There is no point source visible in the MSX images although the diffuse emission at A band does extend to this site.

The central group of maser spots (G10.33−0.17 B, Fig. 4c) appears to lie near an embedded cluster with stars in different evolutionary stages. The maser cluster is 3 arcsec east of a bright, extended K-band object. Examination of the K versus $H - K$ diagram shows that this object is much brighter than most of the other K-band objects in the field. There is diffuse K-band emission in this area. An MSX point source appears to be centred on this cluster.

A reddened object lies 2 arcsec east of the maser group in the south of the field (G10.33−0.17 C, Fig. 4d). This source appears to be brighter at K band than most other sources in the field with the same $H - K$ colour.

None of the maser spots lie within the *IRAS* error ellipse (IRAS 18060−2005). Since *IRAS* has an inferior resolution to that of the MSX satellite, the position reported in the *IRAS* PSC is probably the average position of the two MIR sources resolved by MSX.

4.2 G12.68−0.18 (W33B)

This field does not show much activity in the near-infrared (Fig. 5). There do not appear to be any NIR sources that could be associated with the methanol maser – the nearest reddened sources are 13 arcsec away from the maser position. Although there is no diffuse K-band emission in this field, there are an unusual number of K-band objects visible, indicating a possible cluster of embedded stars. There are water masers 13 arcsec away from the methanol maser position. A line of hydroxyl masers 38 arcsec away is presumably too distant to be excited by the same star as the methanol masers. While no *IRAS* point source is reported here, there is an MSX point source centred on the area between the masers. Haschick & Ho (1983) suggest that the W33 complex consists of successive waves of massive star
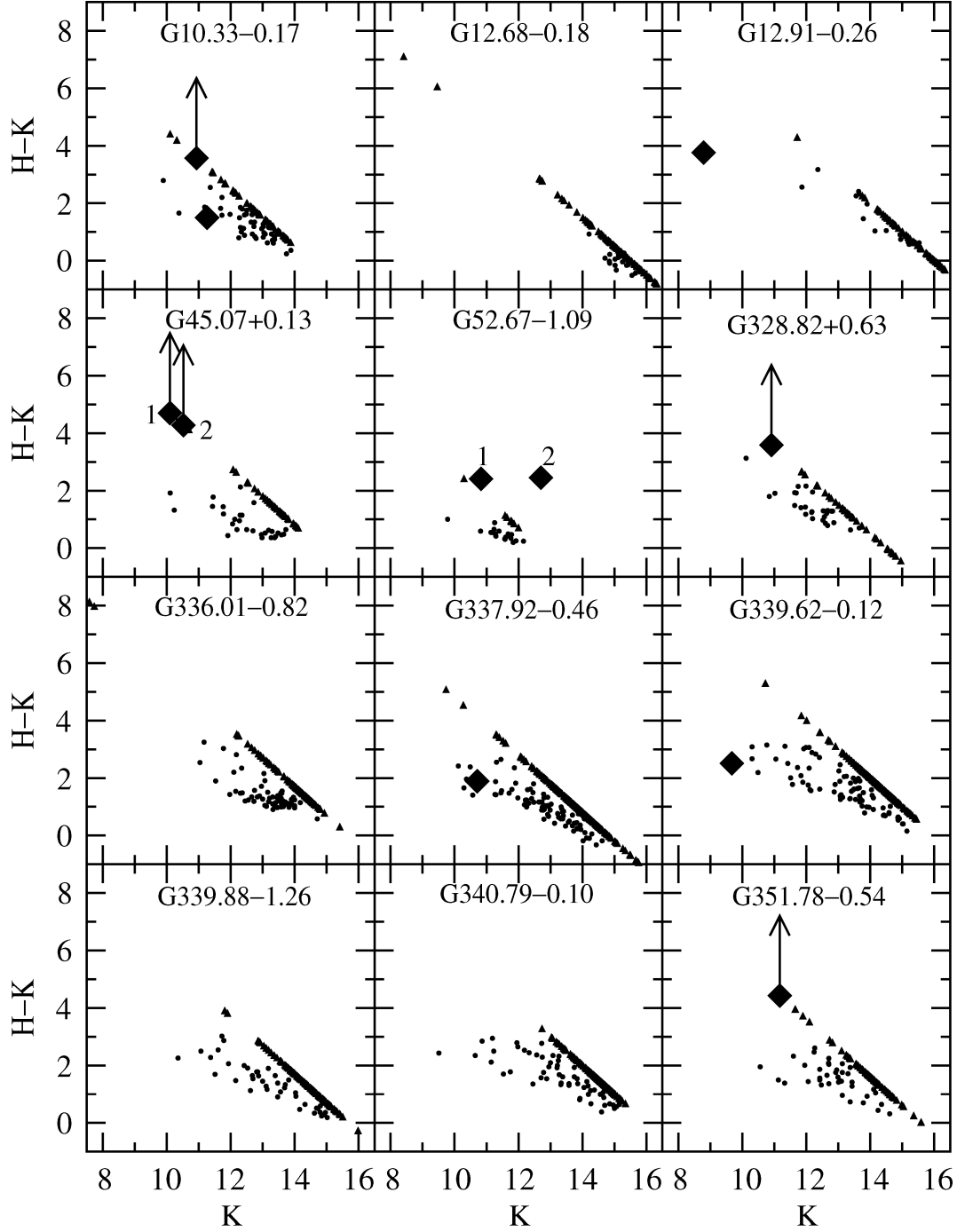
Figure 3. K versus $H - K$ diagram showing sources in all the fields imaged. Only sources detectable at H and K only (filled circles) or K only (filled triangles) are shown. The sources possibly associated with methanol masers are indicated by filled diamonds. The filled triangles and diamonds with arrows indicate that the value plotted is a lower limit for the $H - K$ colour.

formation. They find extended radio emission across the entire complex, while Beiging, Pankonin & Smith (1978) find several compact H II regions clustered within 1 pc of each other.

4.3   G12.91−0.26 (W33A)

All the objects of interest are centred around one NIR source that is visible at J, H and K bands (Fig. 6). This source does not con-

form to the point spread function calculated for the field. Compared with the $H - K$ colour and K magnitude of other sources in this field, this source is very unusual, being the brightest object at K band and having $H - K = 3.8$. Since it is so bright, we have to consider whether the saturation problem found with other bright stars is affecting the results. The J- and H-band magnitudes are too low for there to have been a saturation problem but the K-band magnitude may have been affected. If the K-band flux is greater, this will move the source further to the left in the K versus $H - K$ diagram.

Table 3. Positions of radio sources and references. Single-dish observations are marked with an asterisk. The centroid position is given in cases where multiple maser spot positions were mapped.

Name	Type of source	RA (J2000)	Dec. (J2000)	Pos. unc. (arcsec)	Freq. (GHz)	Ref.
G10.33−0.17	H II region	18 09 01.419	−20 04 30.64	2	5	1
	H II region	18 09 00.323	−20 05 08.42	2	5	1
	H II region	18 08 55.900	−20 05 54.94	2	5	1
	H II region	18 08 58.699	−20 05 21.98	8	4.85	2
	H II region	18 08 58.315	−20 05 15.27	<20	4.85	3
	H II region	18 08 59.000	−20 05 45.00	10*	2.7	4
	Water maser	18 08 55.927	−20 05 53.45	20*	22	5
	Methanol maser C	18 08 55.545	−20 05 57.96	1	6.7	6
	Methanol maser A	18 08 59.988	−20 03 35.56	1	6.7	6
	Methanol maser B	18 09 01.453	−20 05 08.00	1	6.7	6
G12.68−0.18	Water maser	18 13 54.754	−18 01 46.49	0.2	22	7
	Methanol maser	18 13 55.110	−18 01 34.56	10*	6.7	8
	Hydroxyl maser	18 13 54.871	−18 01 45.16	0.5	1.665	9
	H II region	18 13 56.900	−18 00 47.00	10*	8.6	10
G12.91−0.26	Methanol maser	18 13 54.754	−18 01 41.41	1	6.7	6
	Water maser	18 14 39.490	−17 51 59.95	1	22	9
	Hydroxyl maser	18 14 40.250	−17 52 00.07	1	1.665	9
	H II region	18 14 28.920	−17 53 08.10	10*	8.6	10
G45.07+0.13	Methanol maser	19 13 22.130	+10 50 53.92	1	6.7	11
	Water maser	19 13 22.102	+10 50 53.09	<1	22	12
	Hydroxyl maser	19 13 22.034	+10 50 53.81	1	1.665	9
	UC H II region	19 13 21.869	+10 50 48.98	<1	4.9/8.5	13
	UC H II region	19 13 22.080	+10 50 53.20	<1	4.9/8.5	13
G52.67−1.09	Methanol maser	19 32 35.280	+16 57 33.37	60*	6.7	14
	Water maser	19 32 31.670	+16 57 33.20	10*	22	5
G328.81+0.63	Methanol maser	15 55 48.432	−52 43 06.11	1	6.7	6
	Hydroxyl maser	15 55 48.550	−52 43 05.59	1	1.665/1.667	16
	H II region	15 55 48.600	−52 43 08.00	6	4.85	17
G336.01−0.82	Methanol maser	16 35 09.299	−48 46 47.00	1	6.7	6
	Hydroxyl maser	16 35 09.350	−48 46 47.10	1	1.665/1.667	16
	H II region	16 35 05.299	−48 46 12.00	6	4.85	17
G337.91−0.46	Methanol maser	16 41 06.052	−47 07 01.98	1	6.7	6
	Hydroxyl maser	16 41 10.430	−47 08 03.08	1	1.665/1.667	16
	Hydroxyl maser	16 41 06.701	−47 07 02.39	1	1.665/1.667	16
	Water maser	16 41 08.642	−47 07 55.78	20*	22	18
	H II region	16 41 10.601	−47 07 14.99	6	4.85	17
G339.62−0.12	Methanol maser	16 46 05.978	−45 36 43.43	1	6.7	6
	Hydroxyl maser	16 46 06.031	−45 36 43.70	1	1.665/1.667	16
	Water maser	16 46 06.866	−45 36 58.18	10*	22	19
G339.88−1.26	Methanol maser	16 52 04.653	−46 08 33.50	1	6.7	6
	Hydroxyl maser	16 52 04.713	−46 08 30.69	1	1.665	9
	Water maser	16 52 04.637	−46 08 35.16	1	22	9
	UC H II region	16 52 01.682	−46 08 34.40	1	8.5	20
G340.79−0.10	Methanol maser	16 50 14.823	−44 42 26.82	1	6.7	21
	Hydroxyl maser	16 50 14.846	−44 42 22.93	1	1.665/1.667	16
	UC H II region	16 50 14.784	−44 42 21.28	7	8.4	22
G351.78−0.54	Methanol maser	17 26 42.677	−36 09 17.78	1	6.7	23
	Hydroxyl maser	17 26 42.516	−36 09 18.22	1	1.665/1.667	16
	Water maser	17 26 42.329	−36 09 16.38	1	22	9
	UC H II region	17 26 43.459	−36 09 15.80	1	8.64	6
	UC H II region	17 26 42.500	−36 09 17.00	<1	5	24
	UC H II region	17 26 42.460	−36 09 17.60	<1	5	24

Key to references: (1) Becker et al. 1994; (2) Griffith et al. 1994; (3) Kuchar & Clark 1997; (4) Fürst et al. 1990; (5) Brand et al. 1994; (6) Walsh et al. 1998; (7) Lada et al. 1981; (8) Caswell et al. 1995b; (9) Forster & Caswell 1989; (10) Beiging et al. 1978; (11) Phillips C.J., private communication; (12) Hofner & Churchwell 1996; (13) Testi et al. 1999; (14) van der Walt et al. 1996; (15) Palumbo et al. 1994; (16) Caswell 1998; (17) Wright et al. 1994; (18) Scalise & Braz 1980; (19) Batchelor et al. 1980; (20) Ellingsen et al. 1996; (21) Phillips et al. 1998; (22) Argon et al. 2000; (23) Norris et al. 1993; (24) Hughes & MacLeod 1993.

Table 4. Kinematic distances to methanol maser sources. Molecular line velocities are not available for sources marked with an asterisk. In these cases the maser velocity is used. Otherwise the velocities used are the CS(2–1) line velocities (Bronfman et al. 1996).

Object	Adopted velocity (km s^{-1})	Near distance (kpc)	Far distance (kpc)
G10.33−0.17	13.1	2.2	14.5
G12.68−0.18*	55.5	4.9	11.6
G12.91−0.26	36.6	3.9	12.6
G45.07+0.13	59.0	5.1	6.9
G52.67−1.09	59.7	5.1	5.2
G328.81+0.63	−42.3	3.0	11.5
G336.01−0.82	−48.3	3.6	12.0
G337.92−0.46*	−38.5	3.1	12.6
G339.62−0.12	−33.2	2.9	13.0
G339.88−1.26*	−31.6	2.8	13.1
G340.79−0.10*	−105.0	6.0	10.1
G351.78−0.54	−3.4	0.9	16.0

Therefore, even if there are saturation effects, the source is different from other sources in the field.

The methanol maser position falls within the error ellipse of IRAS 18117–1753. The MSX images show a point source centred on the methanol maser position. The water and some of the hydroxyl masers coincide with the methanol maser position. The masers are in a region of the cloud with extended *K*-band emission. It is not clear whether this emission is solely as a result of continuum dust emission since there are only very faint traces of the nebulosity in the *H*-band image and none in the *J*-band image. The emission is elongated and there are two smaller arcs on either side, suggestive of bow shocks. Imaging this area in the shocked molecular hydrogen and Brγ emission bands could determine whether shocks are present. Careful examination of the area in the *H* band shows the presence of other sources in this region. There would appear to be an embedded cluster here, which is consistent with the views of Haschick & Ho (1983) as discussed in the section above.

4.4 G45.07+0.13

The UC H II region, water masers, hydroxyl masers and methanol maser (position given by Chris Phillips, private communication) are clustered on an extended, bright *K*-band source, which is located in the centre of the error ellipse of IRAS 19110+1045 (Fig. 7). An MSX point source is visible at this position. This source is also known to have a bipolar outflow centred in the H II region (Hunter, Phillips & Menten 1997). Another faint *K*-band object 10 arcsec to the south-west (source no 5 in Table 2) is coincident with a UC H II region (Testi, Felli & Taylor 1999) but has no masers associated with it. These two sources are the brightest *K*-band objects in the field.

4.5 G52.67−1.09

The methanol maser position is poorly known since the source position has not been observed with an interferometer. An observation of the maser at Effelsberg (Walsh, private communication) confirms that the position given is accurate to within 1 arcmin. At this level of accuracy, the methanol maser appears to be coincident with the *IRAS* point source position (IRAS 19303+1651, Fig. 8). Observations of the water maser position using the Medicina telescope

(Brand et al. 1994) indicate that the water maser is offset to the west of the *IRAS* position by less than half the Medicina beamwidth of 52 arcsec (Brand, private communication). There are two very faint MSX *A*-band sources visible on either side of the *IRAS* ellipse. There are two highly reddened NIR sources (labelled '1' and '2' in Fig. 8b) 13 arcsec from the maser position. They appear to have $H - K$ colours very different from those of other sources with similar *K* magnitudes. However, until the maser positions are known with higher accuracy, it is not possible to identify potential NIR counterparts to the masers.

4.6 G328.81+0.63

This source has also been imaged at *H* and *K'* by Osterloh et al. (1997). No water masers were detected in this area (Caswell & Haynes 1983). A very bright NIR source is visible 5 arcsec to the north of the methanol maser position (Fig. 9). This is most probably an unrelated source since its spectral energy distribution follows that of a reddened foreground star. A fainter source closer to the maser position is almost lost in the glare from the bright source. This source can be seen more clearly in the *K*-band image of Osterloh et al. (1997). We report the magnitude of the *K*-band object 5 arcsec south of the maser position but this must be regarded as an upper limit since there is contamination from the bright source. A UC H II region is located 2 arcsec to the south of the maser position. It seems that there is a compact embedded cluster here. The error ellipse of IRAS 15520−5234 is centred on the maser positions. The MSX survey shows an unresolved source centred on this position. De Buizer, Piña & Telesco (2000) have imaged this field at mid-infrared wavelengths. They do not see the bright foreground star and so are able to see six embedded stars at 18 μm. They find that the main group of methanol masers coincides with a mid-infrared source. It is not clear whether this source is visible at the NIR. Walsh et al. (2001) have imaged a larger field at 20 μm and obtain similar results.

4.7 G336.01−0.82

The error ellipse of IRAS 16313−4840 is centred on an area containing diffuse emission (Fig. 10). The emission from an MSX point source peaks at the *IRAS* position. The methanol maser is 30 arcsec away and outside of the *IRAS* error ellipse, therefore it is not associated with the *IRAS* source. There are no water masers in this region (Scalise, Rodrigues & Mendoza-Torres 1989). The hydroxyl maser coincides with the methanol masers. A very faint *K*-band object appears at this position, but it may be an artefact of the diffraction spikes from a bright source to the northeast. Walsh et al. (1999) do not have a problem with diffraction spikes in their images and they do not see any NIR source at the methanol maser site.

4.8 G337.92−0.46

The error ellipse of IRAS 16374−4701 is centred on a bright cluster of sources approximately 23 arcsec away from the methanol maser position (Fig. 11). There is extended diffuse emission in the *K* and *H* bands. The methanol masers and a hydroxyl maser are 7 arcsec apart and lie on either side of a faint extended reddened source. The *K* versus $H - K$ colour of this source is not significantly different from several other sources in the field. The only compact H II region observed in the area is 40 arcsec to the east of the methanol maser position. There is another centre of activity to the south with a water maser about 15 arcsec away from an extended bright *K*-band source

Table 5. Distances between methanol masers and other objects in the fields. The methanol maser identity is listed in column 1. The angular separation between field objects and the methanol maser, and its uncertainty, are given in columns 3 and 4. In columns 5 and 6 the projected separation and uncertainty based on the near kinematic distances of the methanol masers are given.

Methanol maser	Object	A. sep (arcsec)	σ (arcsec)	P. sep (kau)	σ (kau)	Methanol maser	Object	A. sep (arcsec)	σ (arcsec)	P. sep (kau)	σ (kau)
G10.33−0.17 A	H II region	59	2	129	4	G12.91−0.26	Hydroxyl maser	10	1	40	4
	H II region	93	2	204	4		Water maser	1	1	2	4
	H II region	151	2	332	4		H II region	69	10	268	39
	H II region	102	8	225	18		K-band object	2	1	6	4
	H II region	132	20	290	44	G45.07+0.13	Water maser	1	1	5	5
	H II region	130	10	286	22		Hydroxyl maser	1	1	7	5
	Water maser	149	20	328	44		H II region	1	1	5	5
	K band A	4	1	10	2		K-band object	2	1	9	5
	K band B	94	1	208	2		K-band object	5	1	26	5
	K band C	154	1	339	2	G52.67−1.09	Water maser	52	60	264	306
	G10.33−0.17 B	95	1	208	2		K-band object	13	60	68	306
	G10.33−0.17 C	155	1	342	2		K-band object	13	60	66	306
G10.33−0.17 B	H II region	37	2	82	4	G328.81+0.63	H II region	2	6	7	18
	H II region	16	2	35	4		Hydroxyl maser	1	1	4	3
	H II region	91	2	201	4		K-band object	5	1	16	3
	H II region	45	8	99	18	G336.01−0.82	Hydroxyl maser	1	1	2	4
	H II region	79	20	174	44		H II region	53	6	190	22
	H II region	51	10	111	22		K-band object	0.5	1	2	4
	Water maser	90	20	198	44	G337.92−0.46	Hydroxyl maser	7	1	22	3
	K band A	98	1	216	2		H II region	48	6	149	19
	K band B	3	1	6	2		Water maser	60	20	186	62
	K band C	95	1	208	2		K-band object	4	1	12	3
	G10.33−0.17 A	95	1	208	2	G339.62−0.12	Water maser	17	20	51	58
	G10.33−0.17 C	97	1	214	2		Hydroxyl maser	1	1	2	3
G10.33−0.17 C	H II region	120	2	265	4		K-band object	2	1	7	3
	H II region	84	2	184	4	G339.88−1.26	Hydroxyl maser	3	1	8	3
	H II region	6	2	13	4		Water maser	2	1	5	3
	H II region	58	8	127	18		H II region	2	1	5	3
	H II region	24	20	52	44		K-band object	2	1	6	3
	H II region	50	10	111	22	G340.79−0.10	H II region	6	1	33	24
	Water maser	7	20	15	44		Hydroxyl maser	4	1	23	6
	K band A	160	1	352	2	G351.78−0.54	Hydroxyl maser	2	1	2	1
	K band B	100	1	219	2		Water maser	4	1	4	1
	K band C	3	1	6	2		H II region	10	1	9	1
	G10.33−0.17 A	155	1	342	2		K-band object	5	1	5	1
	G10.33−0.17 B	97	1	214	2		H II region	2	1	2	1
G12.68−0.18	Water maser	13	10	53	49		H II region	3	1	2	1
	Hydroxyl maser	38	10	188	49						
	H II region	51	10	240	49						

and another hydroxyl maser on the edge of the extended source. The MSX images show an area with extended emission at all bands. The mid-infrared emission is most intense at the *IRAS* position but it appears that there are multiple unresolved sources.

4.9 G339.62−0.12

The methanol and hydroxyl masers overlap in position and are at the edge of a bright NIR source (visible at K and H bands) with extended K-band emission (Fig. 12). Compared with other sources in the field with similar $H - K$ colour, this source is the brightest at K band. The water maser does not appear to be close to any reddened objects but its position is obtained from single-dish observations (Batchelor et al. 1980), therefore the position is not as accurate as from an interferometer. All the masers fall within the error ellipse of IRAS 16424−4531. The peak emission of the MSX point source corresponds to the position of the NIR source.

4.10 G339.88−1.26

The methanol maser is in a very crowded area with a lot of diffuse K-band emission. It is just outside of the error ellipse of IRAS 16484−4603 (Fig. 13). Extended emission at all MSX bands is seen in this area. A bright source is visible in all three bands at the methanol maser position but careful examination of the colour composite image shows a red arc north of the bright star. This is most probably an embedded K-band source that is partially obscured by the bright star in front of it. De Buizer et al. (2002) have imaged this source at mid-infrared wavelengths, where the bright foreground source is not visible. They see an elongated source following the same alignment as the methanol masers. Walsh et al. (1999) find an elongated object at the L band at this position. A UC H II region appears to be centred on the bright NIR source [note that there is an error in the table reporting the position in Ellingsen et al. (1996)]. The hydroxyl and methanol masers lie on the other side of the NIR source. There is a water maser 4 arcsec south of the K-band source.
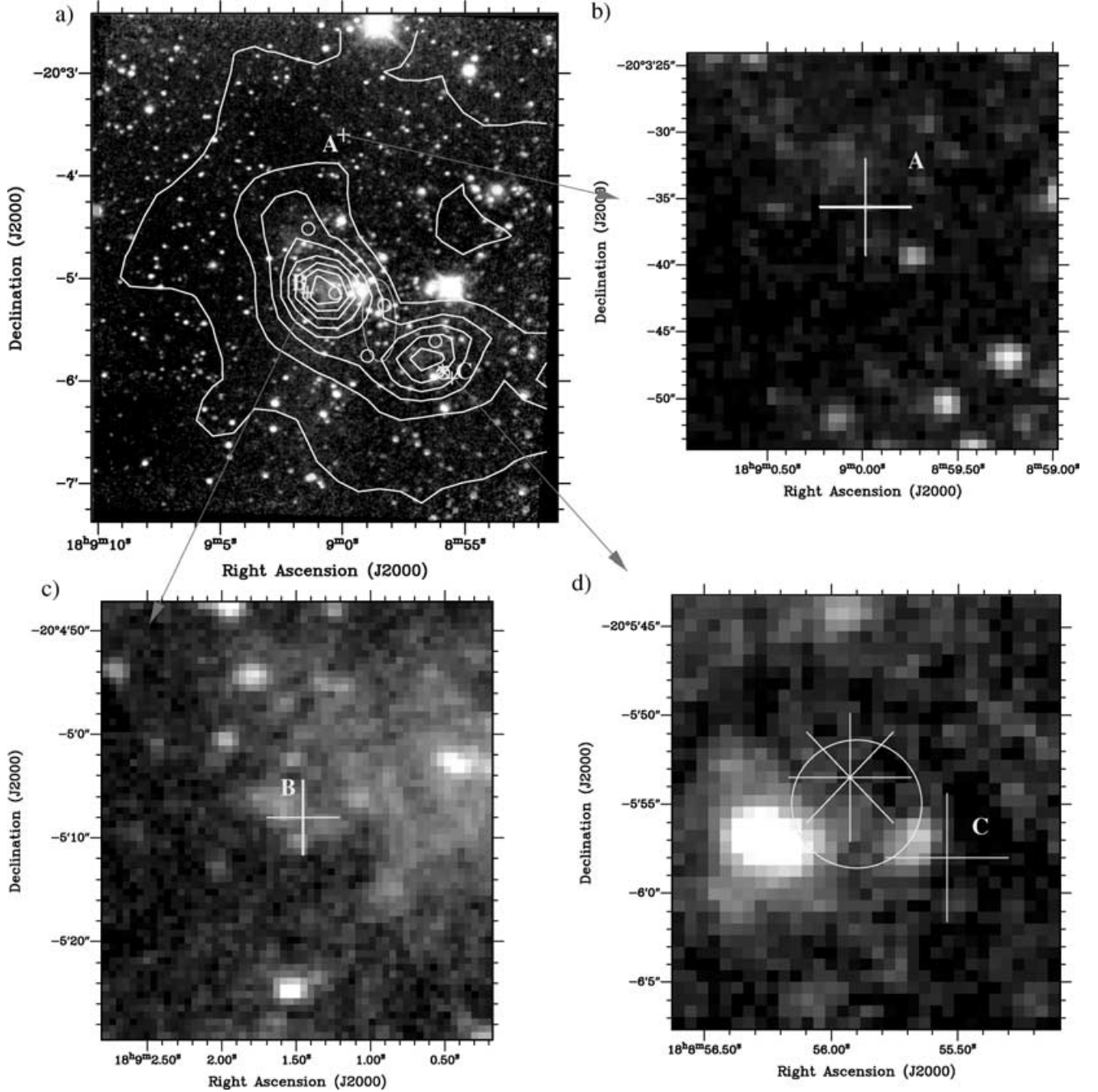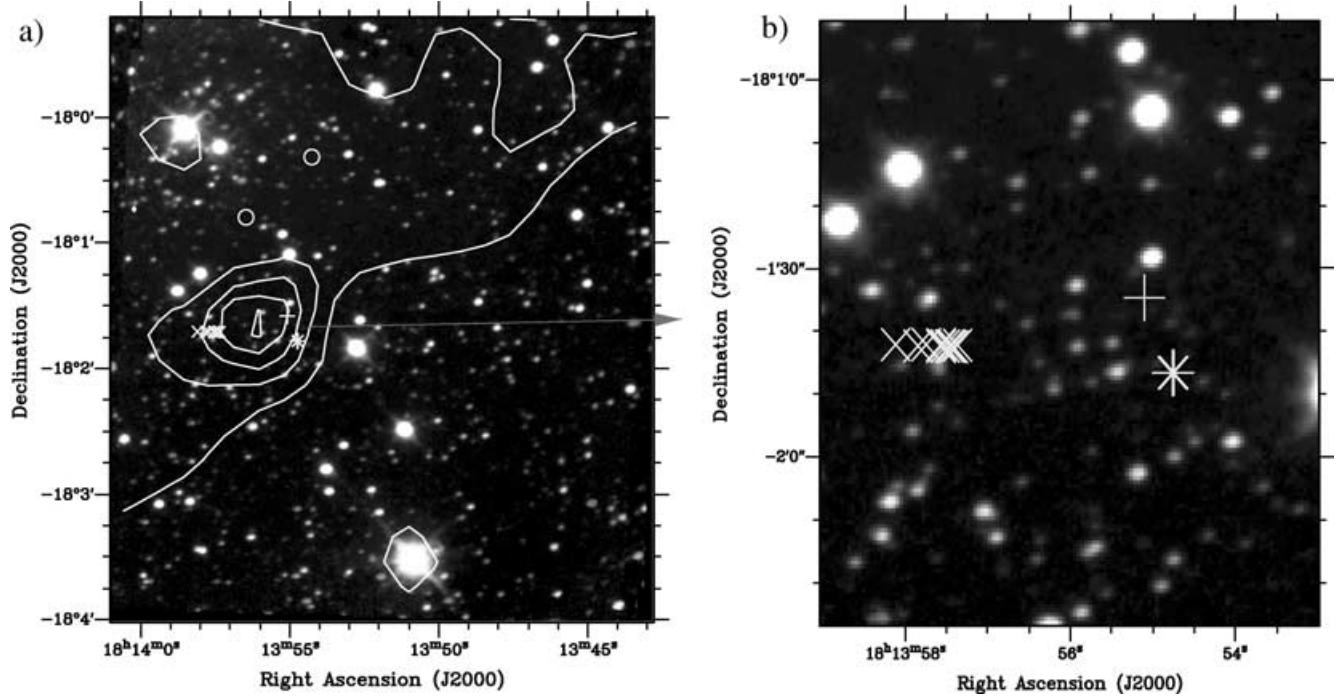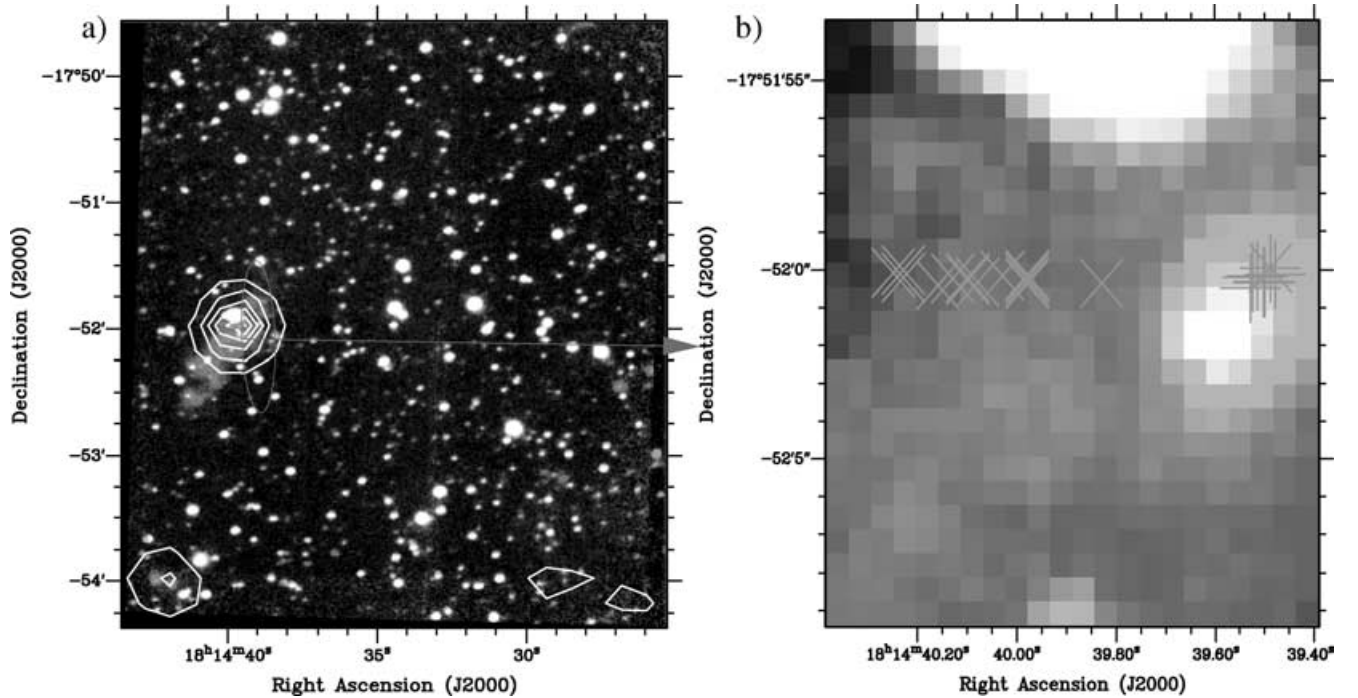
Figure 4. (a) Three-colour composite image of the full field around G10.33−0.17. The known H II regions are marked with ○, water masers with *, 6.7-GHz methanol masers with + and hydroxyl masers with ×. (b) Area around the methanol maser G10.33−0.17 A. (c) Area around the methanol maser G10.33−0.17 B. (c) Area around the water maser, methanol maser G10.33−0.17 C and H II region. This figure is available in colour on *Synergy*, in the online version of this journal.

4.11 G340.79−0.10

The H II region, hydroxyl masers and methanol masers are situated in a region well away from IRAS 16466−4437 (Fig. 14). The only infrared sources visible within 15 arcsec have blue colours similar to that of other field stars in the region. Walsh et al. (1999) also do not detect any reddened objects here. The *IRAS* error ellipse is on the edge of an MSX source. However, examination of the larger MSX field shows that the masers and H II region are at the edge of a dark region in the *A* band. Egan et al. (1998) suggest that these regions

are areas of absorption seen against the infrared-bright background of the galactic plane. These regions are possibly extremely dense, cold dust clouds (Carey et al. 1998).

4.12 G351.78−0.54

The methanol, water and hydroxyl masers are offset from the position of IRAS 17233−3606 (Fig. 15). The active star formation region appears to be in an area with high dust extinction since the

Figure 5. (a) Three-colour composite image of the full field around G12.68−0.18. The known H II regions are marked with ○, water masers with ∗, 6.7-GHz methanol masers with + and hydroxyl masers with ×. (b) Area around the methanol maser. This figure is available in colour on *Synergy*, in the online version of this journal.
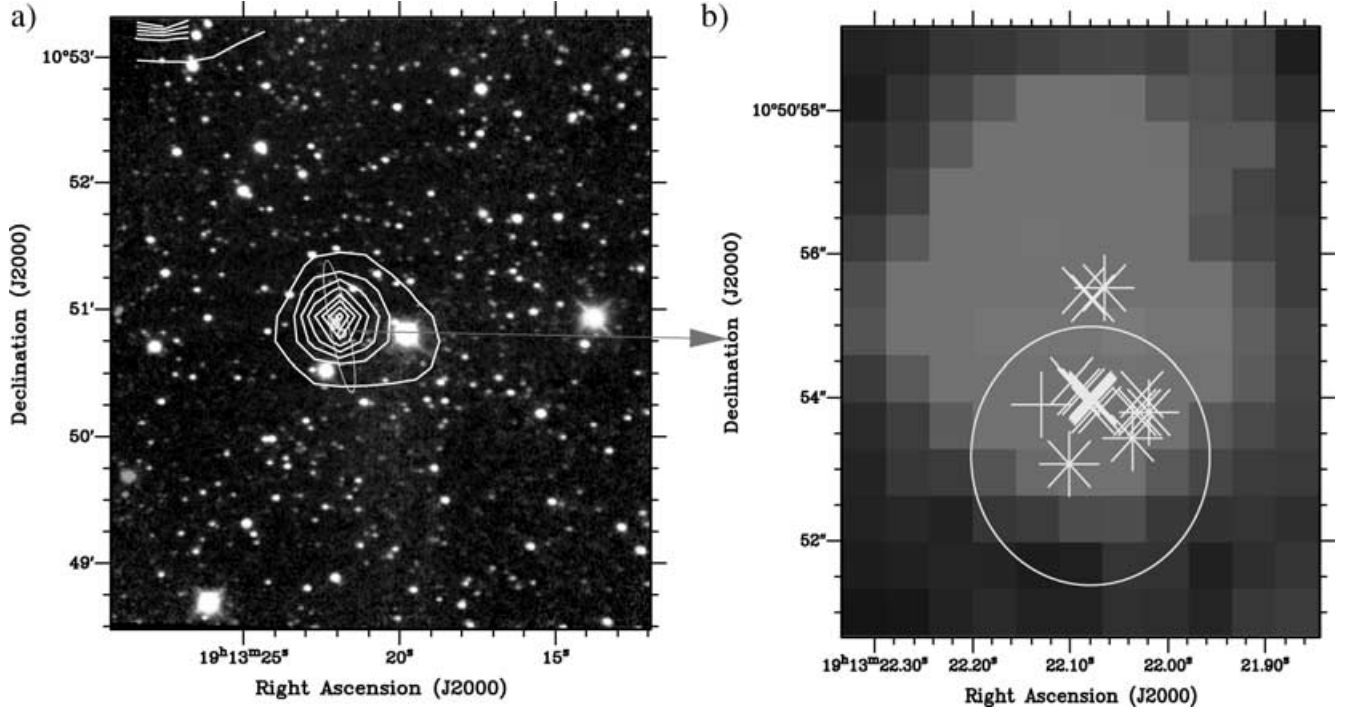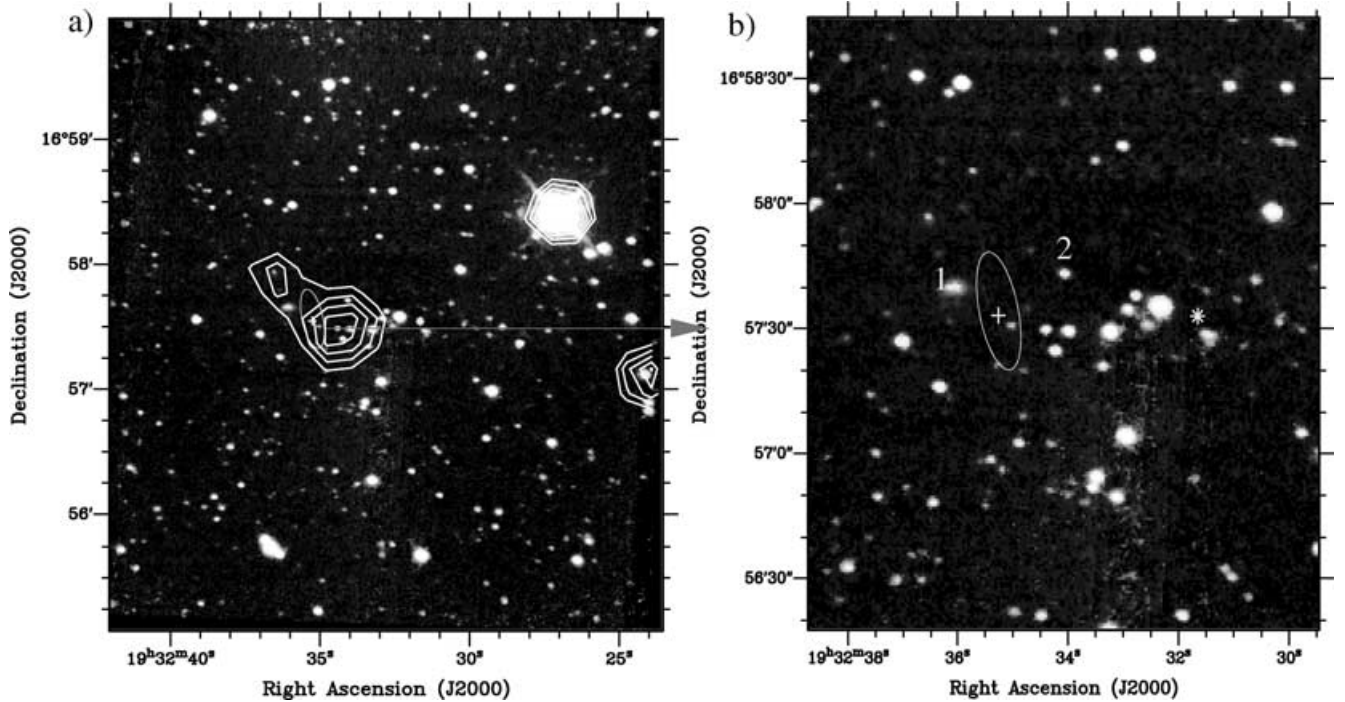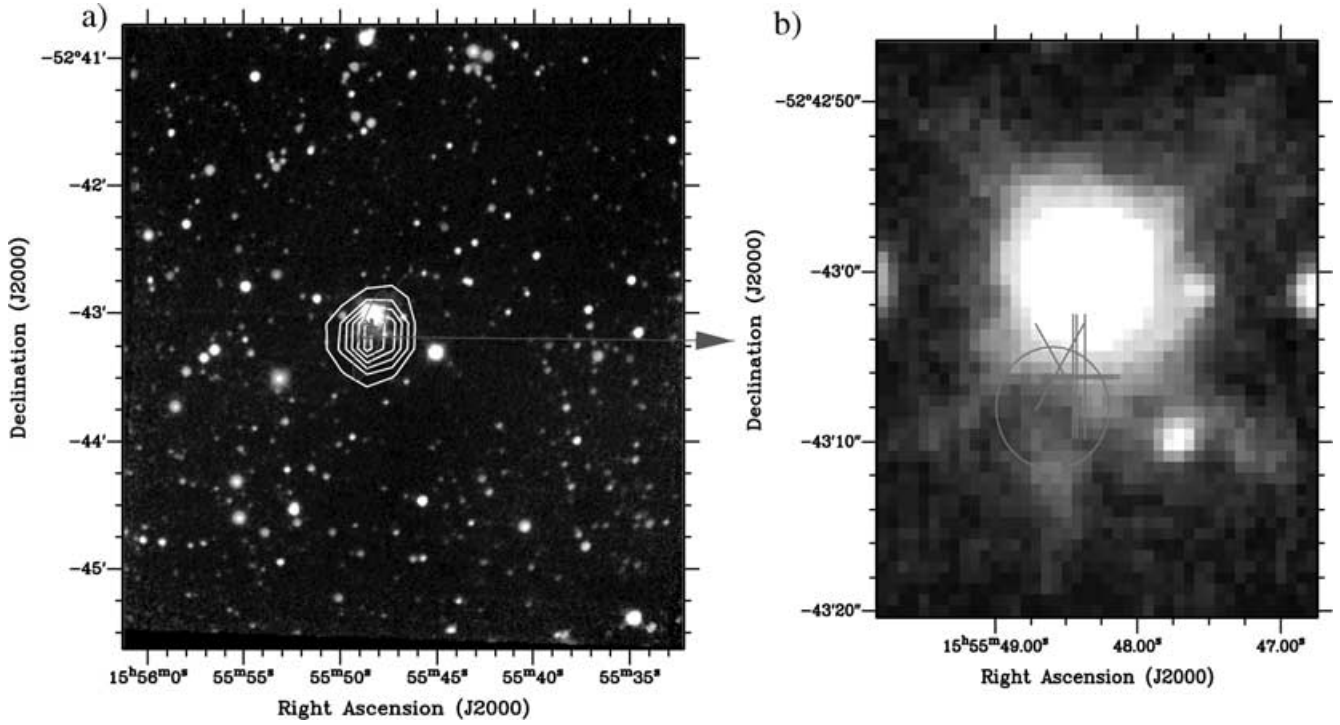

Figure 6. (a) Three-colour composite image of the full field around G12.91−0.26. The known H II regions are marked with ○, water masers with ∗, 6.7-GHz methanol masers with + and hydroxyl masers with ×. (b) Area around the methanol maser. This figure is available in colour on *Synergy*, in the online version of this journal.
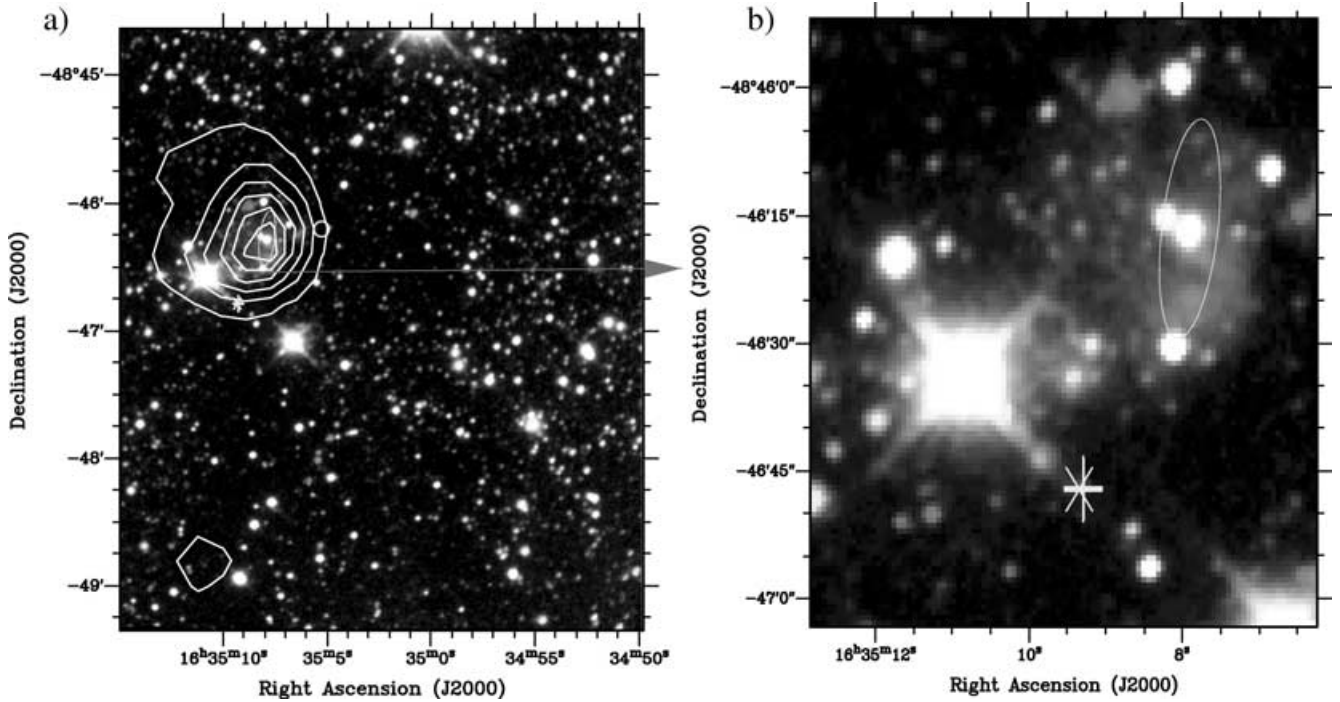
Figure 7. (a) Three-colour composite image of the full field around G45.07+0.13. The known H II regions are marked with ○, water masers with ∗, 6.7-GHz methanol masers with + and hydroxyl masers with ×. (b) Area around the methanol maser. This figure is available in colour on *Synergy*, in the online version of this journal.
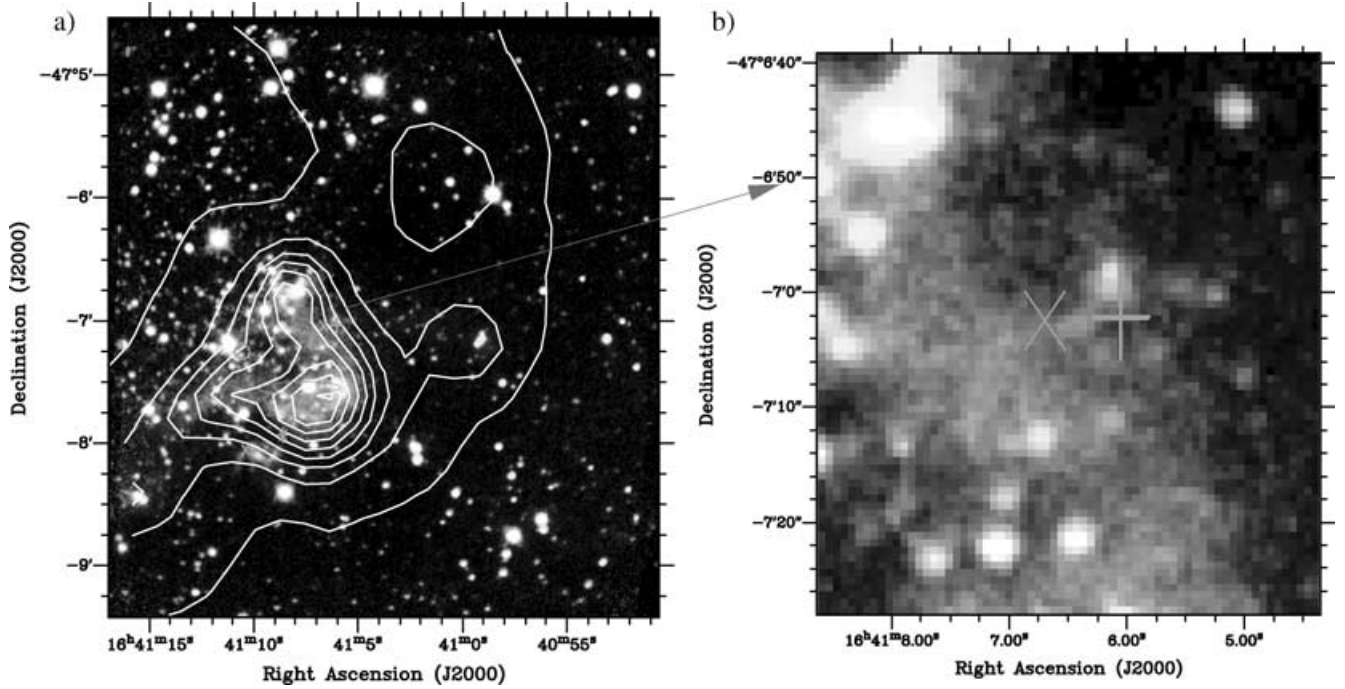

Figure 8. (a) Three-colour composite image of the full field around G52.67−1.09. The known H II regions are marked with ○, water masers with ∗, 6.7-GHz methanol masers with + and hydroxyl masers with ×. (b) Area around the methanol maser. The numerals indicate the sources for which photometry is given in Table 2. This figure is available in colour on *Synergy*, in the online version of this journal.

Figure 9. (a) Three-colour composite image of the full field around G328.81+0.63. The known H II regions are marked with ∘, water masers with ∗, 6.7-GHz methanol masers with + and hydroxyl masers with ×. (b) Area around the methanol maser. This figure is available in colour on *Synergy*, in the online version of this journal.
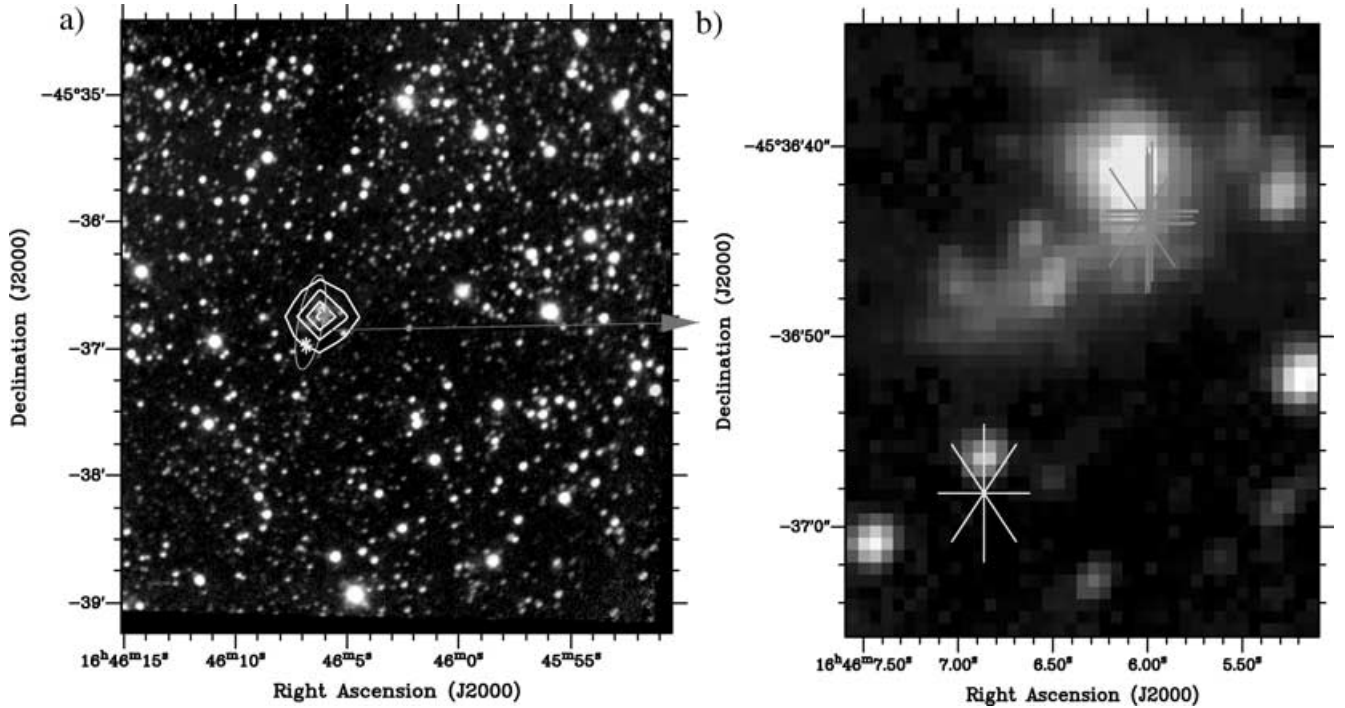

Figure 10. (a) Three-colour composite image of the full field around G336.01−0.82. The known H II regions are marked with ∘, water masers with ∗, 6.7-GHz methanol masers with + and hydroxyl masers with ×. (b) Area around the methanol maser. This figure is available in colour on *Synergy*, in the online version of this journal.
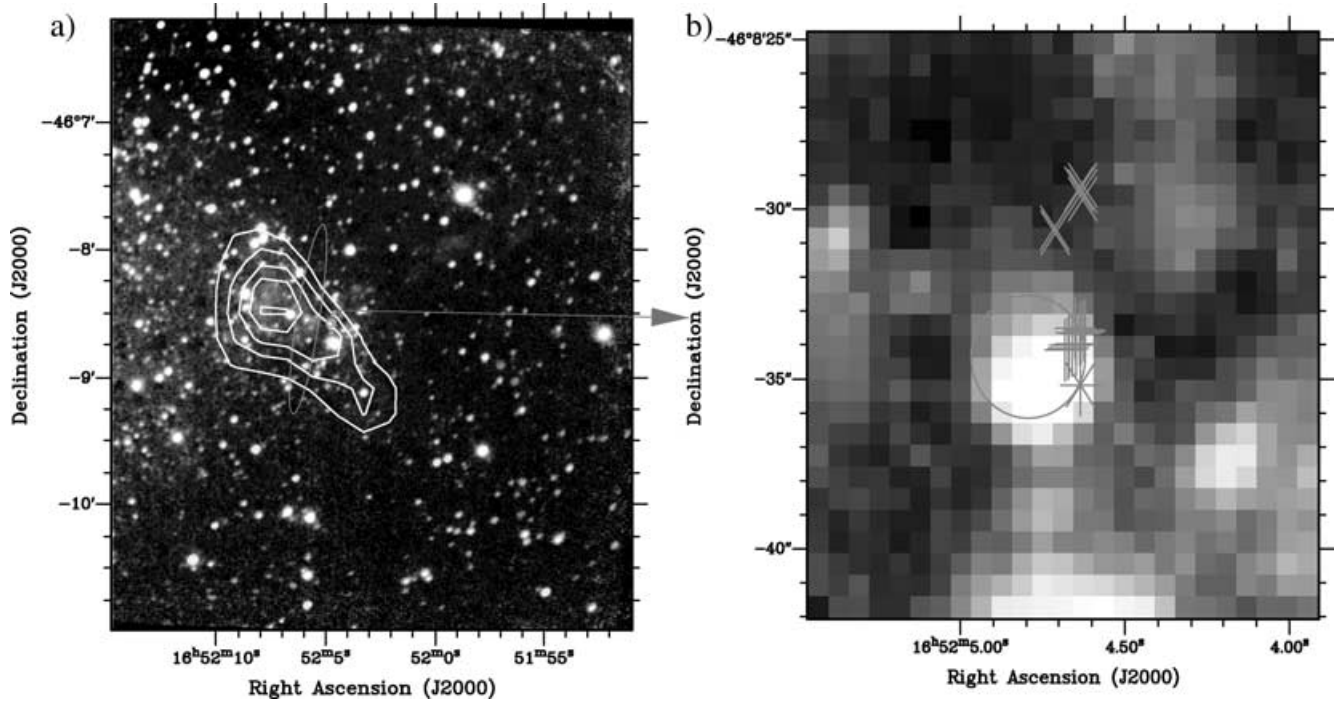
Figure 11. (a) Three-colour composite image of the full field around G337.92−0.46. The known H II regions are marked with ○, water masers with ∗, 6.7-GHz methanol masers with + and hydroxyl masers with ×. (b) Area around the methanol maser. This figure is available in colour on *Synergy*, in the online version of this journal.

Figure 12. (a) Three-colour composite image of the full field around G339.62−0.12. The known H II regions are marked with ○, water masers with ∗, 6.7-GHz methanol masers with + and hydroxyl masers with ×. (b) Area around the methanol maser. This figure is available in colour on *Synergy*, in the online version of this journal.
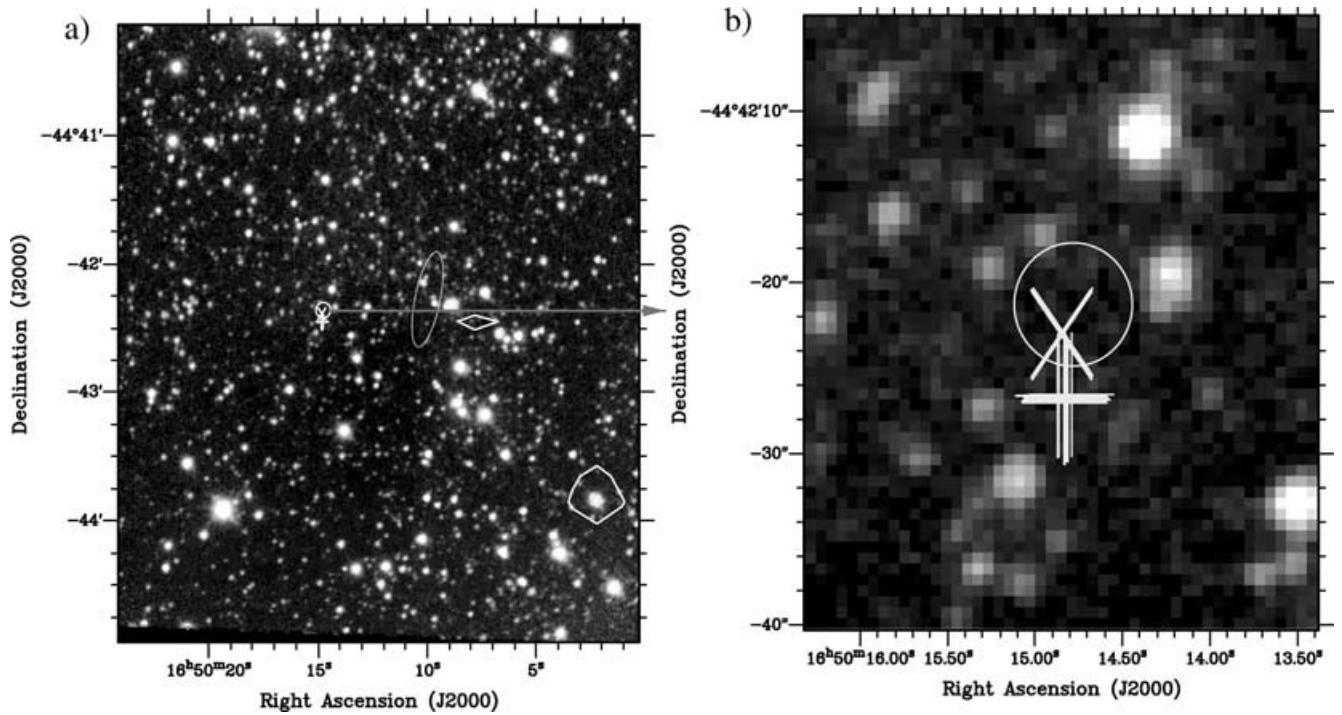
Figure 13. (a) Three-colour composite image of the full field around G339.88−1.26. The known H II regions are marked with ○, water masers with ∗, 6.7-GHz methanol masers with + and hydroxyl masers with ×. (b) Area around the methanol maser. This figure is available in colour on *Synergy*, in the online version of this journal.
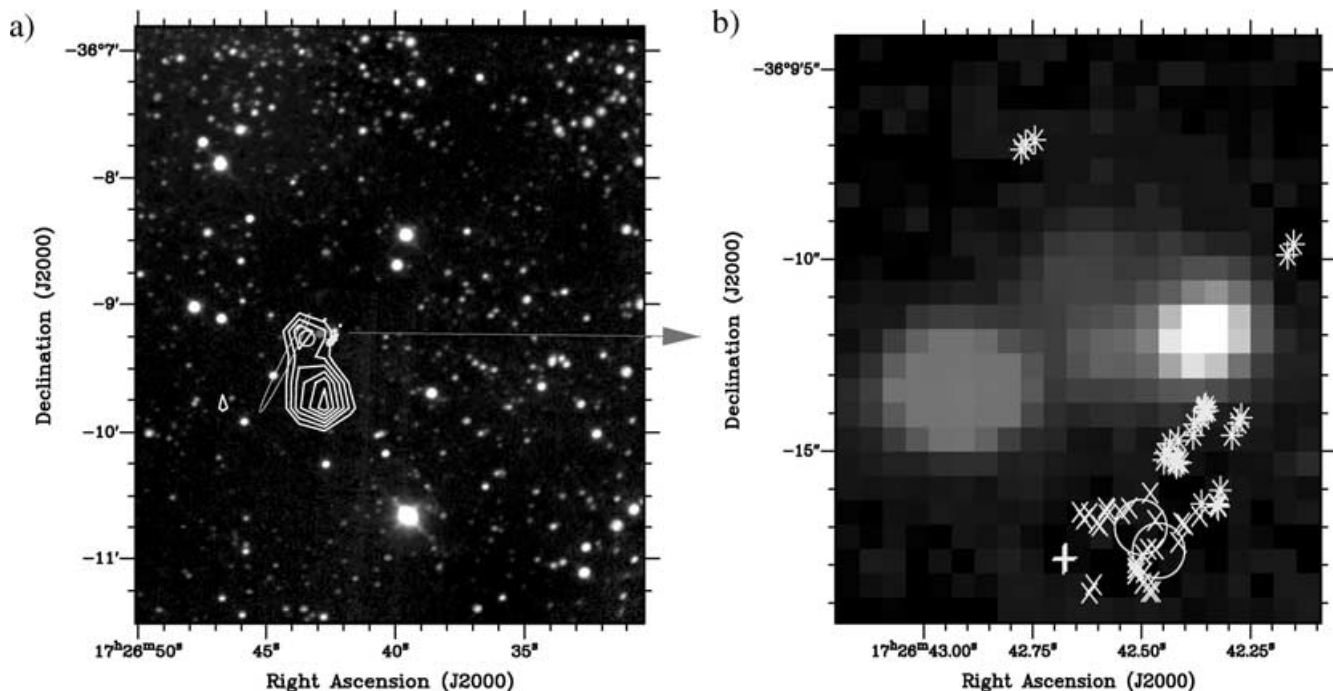

Figure 14. (a) Three-colour composite image of the full field around G340.79−0.10. The known H II regions are marked with ○, water masers with ∗, 6.7-GHz methanol masers with + and hydroxyl masers with ×. (b) Area around the methanol maser. This figure is available in colour on *Synergy*, in the online version of this journal.

Figure 15. (a) Three-colour composite image of the full field around G351.78−0.54. The known H II regions are marked with ○, water masers with ∗, 6.7-GHz methanol masers with + and hydroxyl masers with ×. (b) Area around the methanol maser. This figure is available in colour on *Synergy*, in the online version of this journal.

source density is much lower than in other parts of the field. The MSX images show two unresolved point sources near, but not co-incident with, the methanol masers. A dark filament in the MSX *A* band can be seen in this area. The position of the filament is consistent with the absence of reddened sources in that part of the field. There are two bright NIR sources with some diffuse emission close to the methanol maser position. The eastern source is only visible in the *K* band while the western source has a bluer colour, making it unlikely to be a source in an early evolutionary stage. There is faint nebulosity in the *K* band between the two NIR sources. Walsh et al. (1999) find that the eastern source has an *L*-band counterpart. There are many groups of water masers, northwest of two UC H II regions. The hydroxyl masers are coincident with the H II regions while the methanol masers lie 2 arcsec east of them. The large number of water and hydroxyl masers near these H II regions seems to indicate that there may be other stars even more deeply embedded than the sources that are detected in the NIR.

5   DISCUSSION

5.1   Association of methanol masers with near-infrared objects

Care has to be taken when deciding whether the infrared objects seen near the position of the methanol masers have any causal relationship to the masers. We selected the infrared sources that have colours characteristic of deeply embedded objects. However, it is possible that the object that is pumping the methanol maser is even more deeply embedded or in the hot core stage, in which case we would only be able to detect it at mid-infrared wavelengths. This possibility cannot be eliminated until the fields are imaged with high resolution in the mid-infrared as well.

An upper limit has to be set on the distances that objects can be from each other and still be related to the same star. The largest radius of the spherical UC H II regions mapped by Kurtz, Churchwell & Wood (1994) is approximately 8 kau, while the smallest radius reported is 0.2 kau. A recent mid-infrared image of the site of a UC H II region (De Buizer et al. 2002) shows a hot molecular core with a physical diameter just over 7 kau. If these distances are used as an indicator of the sphere of influence of a newly formed massive star, we can assume that methanol masers more than 8 kau from the star are not associated with it. The projected distance has to be calculated for each object since this is dependent on the distance.

The sources listed in Table 2 satisfy the colour and distance criteria, but they may be chance associations with other embedded stars in the star formation region. In the majority of the cases, the infrared source closest to the methanol maser is among the brightest *K*-band objects in the entire field. This increases the probability that we do not have a chance association. The unusually high *K*-band flux density could be a result of line emission from shocked molecular hydrogen at 2.122 μm. This can only be verified by using narrow-band imaging or spectroscopy. Some of the sources (G10.33−0.17B, G12.91−0.26, G45.07+0.13 and G339.62−0.12) do not follow the point spread function derived using DAOPHOT on other field stars. The nature of these objects is not clear at the resolution obtained in this work. There may be multiple unresolved sources or the object may have a non-spherical morphology, possibly as a result of the presence of outflows or a circumstellar disc.

One way to check for a causal relationship between the NIR object and the maser would be to monitor the infrared radiation from the star while monitoring the methanol maser. If the maser is being pumped by the infrared radiation from the star, then we would expect to see a correlation between the variations in intensity of the objects.

5.2 Relation of methanol masers to other star formation tracers

The positions of H II regions, hydroxyl masers and water masers can tell us more concerning the environment of the methanol masers. The existence of an H II region is a sure indicator of the presence of a high-mass ionizing star. Hydroxyl masers are found at the edges of compact H II regions (Garay, Reid & Moran 1985), and are a good indicator of the presence of a high-mass star even when the H II region may not be detectable. Water masers are found in shocks associated with high-velocity outflows. However, water masers are associated with both high- and low-mass star formation and may be found some distance from the star driving the outflow, making it difficult to verify the association without actually mapping the outflows.

We can assume, as discussed in the previous section, that objects with a separation of more than 8 kau are not likely to be causally related. Table 4 shows the distances used to calculate the projected separations between the methanol maser source and other objects (Table 5). These separations are a lower value only, since we are using the near kinematic distance and we do not know the distance between the objects along the line of sight. In this discussion, the methanol maser is used as the reference point, rather than the possible NIR counterparts since we cannot be sure that these stars are related to the methanol maser.

Fig. 16 shows the relation between the methanol maser sources and other radio sources. All of the sources in this sample, except for G52.67−1.09, have been targeted by searches for compact H II regions, water masers and hydroxyl masers. Only G10.33−0.17 A, G10.33−0.17 B and G337.92−0.46 have no detectable compact H II regions (confirmed for G10.33−0.17 by a recent VLA observation by van der Walt et al. 2002) or other maser species associated with them. Since G12.68−0.18 and G12.91−0.26 are in the extended H II region complex W33 (Beiging, Pankonin & Smith 1978), it is possible that the higher noise levels make it difficult to detect weak

compact H II regions. The majority of the methanol maser sources are close to compact H II regions or hydroxyl masers, indicating the presence of a massive star. There are no methanol maser sources associated with an H II region without the presence of other maser species, which is consistant with the hypothesis that the methanol masers are associated with an early evolutionary phase of the star.

5.3 MSX and *IRAS* sources

In the past, many researchers have used *IRAS* colours as selection criteria to find methanol masers or H II regions. Yet not all methanol masers appear to be associated with *IRAS* sources (Ellingsen et al. 1996). In our sample, eight out of 14 methanol maser sites are not within the *IRAS* error ellipse. However, far-infrared sources may be excluded from the *IRAS* point source catalogue because of confusion in densely populated areas. The higher-resolution MSX survey gives a better incidence of methanol masers found within the contours of an MSX point source.

In comparison with *IRAS*, only two methanol masers (G10.33−0.17 A and G340.79−0.10) are not coincident with MSX sources. In many cases it is clear that the *IRAS* PSC is simply selecting the area of brightest infrared emission or is unable to distinguish between multiple sources. The MSX survey specifically targeted areas that *IRAS* marked as confused, as well as the entire Galactic plane. Therefore, the MSX survey is a better tool to use when searching for potential infrared counterparts to methanol masers. However, the resolution and positional accuracy of MSX makes it impossible to identify the individual stars that are exciting the masers.

6 SUMMARY

We have imaged 12 fields around methanol maser sources in the *I*, *J*, *H* and *K* bands. Seven of the methanol masers sites are within 8 kau of a near-infrared source with colours characteristic of a deeply embedded star. In many cases these sources are amongst the brightest *K*-band sources in the field. Some of these sources are not point sources.

The crowded nature of the star formation regions makes it difficult to be certain that we have identified the star exciting the methanol masers. High-resolution observations at longer wavelengths are needed to identify objects that may be more deeply embedded. Monitoring the infrared source and the methanol masers to check for correlations in variability may be a way to test the association of the sources.
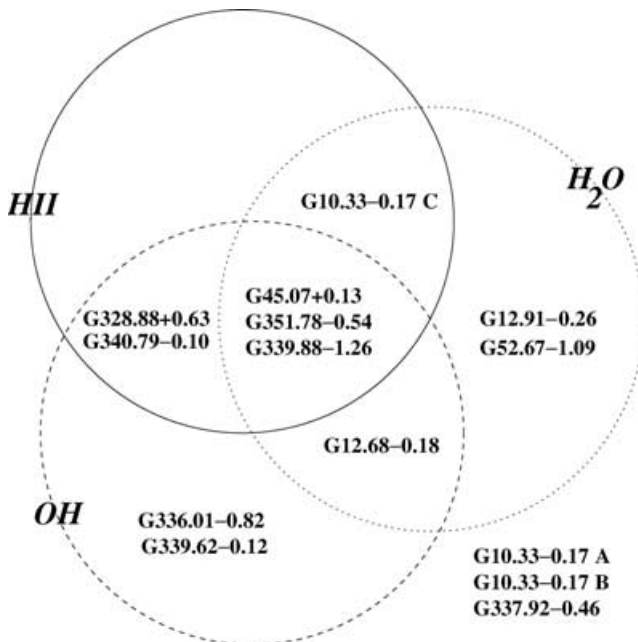
Figure 16. Venn diagram showing the association of methanol maser sources with other radio sources. The sources placed outside the circles are not associated with any other type of radio source.

REFERENCES

Argon A. L., Reid M. J., Menten K. M., 2000, ApJS, 129, 159
Batchelor R. A., Caswell J. L., Goss W. M., Haynes R. F., Knowles S. H., Wellington K. J., 1980, Aust. J. Phys., 33, 139
Becker R. H., White R. L., Helfand D. J., Zoonematkermani S., 1994, ApJS, 91, 347
Beiging J. H., Pankonin V., Smith L. F., 1978, A&A, 341, 341
Brand et al., 1994, A&AS, 103, 541

Bronfman L., Nyman L. A., May J., 1996, A&AS, 115, 81

Carey S. J., Clark F., Egan M., Price S., Shipman R., Kuchar T., 1998, ApJ, 508, 721

Carpenter J. M., 2001, ApJ, 121, 2851

Caswell J. L., 1998, MNRAS, 297, 215

Caswell J. L., Haynes R. F., 1983, Aust. J. Phys, 36, 361

Caswell J. L., Vaile R. A., Ellingsen S. P., Norris R. P., 1995, MNRAS, 274, 1126

Caswell J. L., Vaile R. A., Ellingsen S. P., Whiteoak J. B., Norris R. P., 1995, MNRAS, 272, 96

Cohen M., Walker R., Barlow M., Deacon J., 1992, AJ, 104, 1650

De Buizer J. M., Piña R. K., Telesco C. M., 2000, ApJS, 130, 437

De Buizer J. M., Walsh A. J., Piña R. K., Phillips C. J., Telesco C. M., 2002, ApJ, 564, 327

De Buizer J. M., Watson A. M., Radomski J. T., Piña R. K., Telesco C. M., 2002, ApJ, 564, L101

Egan M., Shipman R., Price S., Carey S., Clark F. O., Cohen M., 1998, ApJ, 494, L199

Ellingsen S. P., von Bibra M. L., McCulloch P. M., Norris R. P., Deshpande A. A., Phillips C. J., 1996, MNRAS, 280, 378

Forster J. R., Caswell J. L., 1989, A&A, 213, 339

Fürst E., Reich W., Reich P., Reif K., 1990, A&AS, 85, 805

Garay G., Lizano S., 1999, PASP, 111, 1049

Garay G., Reid M., Moran J., 1985, ApJ, 289, 681

Goedhart S., van der Walt D., Schutte A., 2000, MNRAS, 316, 316

Gooch R., 1996, PASA, 14, 106

Griffith M. R., Wright A. E., Burke B., Ekers R. D., 1994, ApJS, 90, 179

Haschick A. D., Ho P. T. P., 1983, ApJ, 267, 638

Hofner P., Churchwell E., 1996, A&AS, 120, 283

Hughes V., MacLeod G., 1993, AJ, 105, 1495

Hunter T. R., Phillips T. G., Menten K. M., 1997, ApJ, 478, 283

IRAS, 1985, IRAS Point Source Catalog. US Government Printing Office, Washington, DC

Koorneef J., 1983, A&A, 128, 84

Kuchar T. A., Clark F. O., 1997, ApJ, 488, 224

Kurtz S., Churchwell E., Wood D. O. S., 1994, ApJS, 91, 659

Lada C. J., Adams F. C., 1992, ApJ, 393, 278

Lada C. J., Blitz L., Reid M. J., Moran J. M., 1981, ApJ, 243, 769

Leitherer C., Robert C., Drissen L., 1992, ApJ, 401, 596

Minier V., Booth R. S., Conway J. E., 2000, A&A, 362, 1093

Minier V., Conway J. E., Booth R. S., 2001, A&A, 369, 278

Norris et al., 1998, ApJ, 508, 275

Norris R. P., Whiteoak J. B., Caswell J. L., Wieringa M. H., Gough R. G., 1993, ApJ, 412, 222

Osterloh M., Henning T., Launhardt R., 1997, ApJS, 110, 71

Palumbo G., Scappinni F., Pareschi G., Codella C., Caselli P., Attolini M., 1994, MNRAS, 266, 123

Persson S. E., Murphy D. C., Krzeminski W., Roth M., Rieke M. J., 1998, AJ, 116, 2475

Phillips C. J., Norris R., Ellingsen S. P., McCulloch P. M., 1998, MNRAS, 300, 1131

Price S. D., Egan M. P., Carey S. J., Mizuno D. R., Kuchar T. A., 2001, AJ, 121, 2819

Rieke G. H., Lebofsky M. J., 1985, ApJ, 288, 618

Scalise E., Braz M. A., 1980, A&A, 85, 149

Scalise E., Rodrigues L., Mendoza-Torres E., 1989, A&A, 221, 105

Testi L., Felli M., Persi P., Roth M., 1994, A&A, 288, 634

Testi L., Felli M., Persi P., Roth M., 1998, A&AS, 129, 495

Testi L., Felli M., Taylor G. B., 1999, A&AS, 138, 71

van der Walt D. J., Retief S. J. P., Gaylard M. J., MacLeod G. C., 1996, MNRAS, 282, 1085

van der Walt D. J., Churchwell E., Gaylard M., Goedhart S., 2002, MNRAS, submitted

Walsh A. J., Burton M. G., Hyland A. R., Robinson G., 1998, MNRAS, 301, 640

Walsh A. J., Burton M. G., Hyland A. R., Robinson G., 1999, MNRAS, 309, 905

Walsh A., Bertoldi F., Burton M., Nikola T., 2001, MNRAS, 326, 36

Wright A. E., Griffith M. R., Burke B. F., Ekers R. D., 1994, ApJS, 91, 111

APPENDIX A: ZERO-MAGNITUDE FLUXES FOR THE LCO SYSTEM

The flux density in Jy at a particular wavelength is given by

$$F_\lambda = F_\lambda^0 10^{-m_\lambda/2.5}, \tag{A1}$$

where F_λ^0 is the flux density at λ of a zero-magnitude star and m_λ is the magnitude at λ. Cohen et al. (1992) give the zero-magnitude flux calibration for the stars Vega and Sirius. However, these fluxes were measured using the UKIRT photometric system. Our source magnitudes are calibrated to the LCO (Persson et al. 1998) photometric system. A direct conversion between the two systems is not available in the literature. However, Carpenter (2001) gives transformation equations for a number of photometric systems (including UKIRT and LCO) to the 2MASS photometric system. It is therefore possible to derive the transformation equations to convert from the UKIRT system to the LCO system. The transformation equations are given below:

$$K_{\mathrm{LCO}} = K_{\mathrm{UKIRT}} + 0.005(J - K)_{\mathrm{UKIRT}} + 0.008 \tag{A2}$$

$$H_{\mathrm{LCO}} = 1.054(H - K)_{\mathrm{UKIRT}} + K_{\mathrm{LCO}} + 0.015 \tag{A3}$$

$$J_{\mathrm{LCO}} = 1.055(J - K)_{\mathrm{UKIRT}} + K_{\mathrm{LCO}} - 0.005. \tag{A4}$$

We can then obtain the flux densities for Vega on the LCO system. Table A1 gives the converted values.

Table A1. Fluxes for Vega on the LCO system.

Filter	λ (μm)	m_λ (mag)	νF_ν (W m^{-2})	F_λ (Jy)
J	1.25	20.90	4.365e−09	1.819e3
H	1.65	21.77	1.959e−09	1.077e3
K	2.2	22.61	9.036e−10	6.626e2

This paper has been typeset from a TEX/LATEX file prepared by the author.